Advanced Materials

ADVANCED MATERIALS
www.advmat.de

RESEARCH ARTICLE

A Scalable, Robust, and Bioinspired Liquid Diode for Ultrafast Unidirectional Absorption

Yonghua Li[1,2] | Ming Li[1,2] | Ximeng Zhang[1,2] | Tianzhi Li[1,2] | Yu-Qiong Luo[1,2] | Xi Yao[1,2] | Lei Jiang[3] | Jie Ju[1,2]

[1]School of Nanoscience and Materials Engineering, Henan University, Zhengzhou, Henan, China | [2]Key Lab for Special Functional Materials, Ministry of Education, Kaifeng, Henan, China | [3]CAS Key Laboratory of Bio-inspired Materials and Interfacial Science, Technical Institute of Physics and Chemistry, Chinese Academy of Sciences, Beijing, China

Correspondence: Yu-Qiong Luo (luo2020start@henu.edu.cn) | Xi Yao (yaoxi@henu.edu.cn) | Jie Ju (jujie@henu.edu.cn)

Received: 4 February 2026 | **Revised:** 12 June 2026 | **Accepted:** 27 August 2026

Keywords: electrostatic flocking | microfiber-covered porous substrate | non-solvent-induced phase separation | scalable | ultrafast unidirectional absorption

ABSTRACT

Efficient management of biofluids on body surfaces is essential for advanced medical protection and healthcare. While conventional designs often rely solely on unidirectional penetration, our previously established model of a microfiber-covered porous substrate leverages synergistic interplay between lateral capillary forces and vertical permeation to enhance absorption kinetics by over 150-fold. However, scalable fabrication and mechanical robustness of such a structure remain challenging. Here, we present a semi-continuous manufacturing strategy based on electrostatic flocking combined with non-solvent-induced phase separation to produce a trilayered composite consisting of a micro-fiber array, a porous adhesive interlayer, and a fibrous support (MA-PA-FS). We systematically elucidate the role of each layer in guiding rapid liquid absorption and enhancing structural integrity. The optimized MA-PA-FS composite achieves ultrafast unidirectional water absorption (5 μL in 9.3 ms)—three orders of magnitude faster than a porous control surface (90.0 s)—and also effectively absorbs viscous biological fluids such as fresh porcine blood. Besides exceptional liquid absorption, the material exhibits high moisture permeability and strong mechanical durability. This study provides a scientific foundation for designing scalable, high-performance biofluid-handling interfaces, with promising potential in medical textiles, protective gear, and related health technologies.

1 | Introduction

The efficient management of biofluids on body surfaces—such as sweat, wound exudate, or blood—is critical for maintaining hygiene, comfort, and health in medical and protective scenarios [1–3]. Materials capable of rapid, unidirectional liquid transport have thus attracted significant interest for applications in wearable electronics [3, 4], functional textiles [5, 6], advanced wound dressings [7–9], and hygiene products [10–12]. Organisms in nature, such as spider silk [13], cactus spine [14], shorebird beak [15], desert beetle [16], and *Araucaria* leaf [17], achieve directional liquid transport through surface free energy or topography gradient. Inspired by nature, a prevailing strategy to enhance unidirectional absorption involves constructing surface free energy or morphological gradients along the vertical axis of porous substrates, thereby augmenting the capillary driving force for liquid penetration [3, 18–22]. While effective, such designs typically emphasize vertical imbibition while overlooking the complementary role of lateral spreading. For instance, for most porous substrates that rely solely on longitudinal driving force, the absorption time of microliter droplets is several seconds [18–23]. In fact, liquid uptake in porous media is governed by the coupled dynamics of in-plane spreading and through-plane imbibition [24–26].

Our previous study focused on the abhymenium (hairy surface) of wood ear (*Auricularia auricula-judae*, a common type of edible fungus), featuring ultrafast, unidirectional liquid absorption. We revealed that its bilayer "micro-hairs atop porous substrate" structure synergizes lateral capillary spreading with vertical imbibition, enhancing absorption rates by more than 150-fold compared to designs relying solely on vertical imbibition [27]. Artificial replicas of this structure, fabricated via lithography template-based replication, further confirmed its superior liquid absorption performance. Nevertheless, with a template-based replication strategy, the limited number of templates severely limits the regulation of fine structures of the composite, and large-scale fabrication of the composite remains challenging. Moreover, the porous replicas prepared by freeze-drying are mechanically weak, fragile, and unfoldable. Therefore, scalable production of a high-performance microfiber-covered porous substrate is critical for the practical application of this superior liquid management strategy.

Electrostatic flocking, a textile technique that aligns and attaches micro-fibers onto adhesive substrates using an electric field [28, 29], offers a promising alternative for large-scale, continuous manufacturing of micro-fiber structured surfaces [28–32]. Unlike other micro-fiber creation techniques, such as soft lithography, high-energy beam machining, surface etching, ultra-precision machining, 3D printing, or template replication, flocking is substrate-versatile and inherently scalable [33–37]. However, conventional flocking yields a dense adhesive film layer after drying, which severely restricts vertical liquid imbibition. In addition to the atop micro-fiber array, a porous sublayer is indispensable for rapid, unidirectional liquid absorption. Non-solvent-induced phase separation (NIPS) is a convenient and simple method to fabricate polymer monoliths with a microporous structure [38–40]. High-performance porous polymer membranes with wide applications such as water desalination [41], bioelectronics [42], and lateral flow immunoassay [43] have been constructed via NIPS. As demonstrated in our previous work, a surface with solely a porous substrate or micro-fiber array exhibits longer liquid absorption time than a microfiber-covered porous substrate. Thus, integrating a micro-pillar array with porous substrate via flocking and NIPS is key to fabricating a composite that enables ultrafast, unidirectional liquid absorption.

Here, we combine continuous electrostatic flocking with in-line NIPS and cross-linking to fabricate a trilayer composite: a microfiber array attached via a porous poly(vinyl alcohol) adhesive layer to a fibrous support (MA-PA-FS). This design not only enables scalable manufacturing but also restores the structural synergy observed in the natural system. The wood ear-mimicking MA-PA-FS, featuring robust mechanical durability, high moisture permeability, and ultrafast unidirectional liquid absorption, holds great promise for advanced biofluids management materials.

2 | Results

2.1 | Fabrication of Micro-Fiber Array-Porous Adhesive Interlayer-Fibrous Support (MA-PA-FS)

Microfiber, porous adhesive, and fibrous support are the basic components of the MA-PA-FS, whose hydrophilicity is essential for the liquid absorption performance of the MA-PA-FS. As shown in Figures S1 and S2, water contact angles (WCAs) of nylon microfiber and poly(vinyl alcohol) (PVA) adhesive are 71.7° ± 9.5° and 65.5° ± 0.9°, respectively, and the non-woven fabric can absorb a 5 μL water droplet within 33.7 s. Those results indicate the hydrophilicity of the three components of the MA-PA-FS. Figure 1a, Figure S3 and Movies S1–S3 show the semi-continuous fabrication process of MA-PA-FS. Non-woven fabric is first blade-coated with PVA solution (Movie S2). Upon application of voltage, short fibers are gradually polarized and fly toward the PVA-coated surface, and finally anchor vertically in the PVA solution (Figure 1b and Movie S3). Then the flocked fabric is immersed in isopropanol, where a solvent (water)-nonsolvent (isopropanol) exchange of PVA takes place. A homogeneous PVA solution separates into a PVA-rich and a PVA-lean phase, leading to the formation of a porous PVA adhesive interlayer [44, 45] (Figure 1c). Thereafter, PVA is crosslinked by glutaraldehyde, and the MA-PA-FS is dried under an infrared heater. Finally, the MA-PA-FS with a width of 4 cm is collected as a roll, demonstrating a great opportunity for scaling up (Figure 1d). The MA-PA-FS consists of three components: upper micro-fiber array, porous PVA interlayer, and fibrous support (Figure 1e). As shown in Figure 1f and Figure S4, vertically aligned microfibers are anchored on the non-woven fabric via the porous PVA interlayer, which is analogous to the "micro-hairs atop porous substrate" structure of the abhymenium of wood ear fungus [27]. It is speculated that for the MA-PA-FS surface, the microstructural mimicry of hairs on the wood ear fungus enables ultrafast liquid absorption by the integration of lateral spreading and vertical imbibition (Figure 1e).

2.2 | Optimization of Fabrication Parameters

The liquid absorption property of the MA-PA-FS is affected by both its microstructure and chemical composition. Thus, the micro-fiber array, porous adhesive layer, and fibrous support are regulated to optimize the liquid absorption time on MA-PA-FS. As shown in Figure 2a, CA∼0 is defined as the moment when the contact angle of the droplet on the top of the microfiber becomes 0°, and the liquid absorption time is the time interval from droplet contact with the sample surface to CA∼0. Commercial short fibers including nylon, viscose, and cotton fiber are selected, with average lengths of 300.3, 302.9, and 311.1 μm, and WCAs of 71.7°, 60.5°, and 129.2°, respectively (Figures S5 and S6). Owing to the hydrophilicity of nylon and viscose fiber, MA-PA-FSs with nylon and viscose fiber exhibit shorter liquid absorption times of 9.3 and 13.1 ms, respectively (Figure 2b). Compared to slightly crimped viscose and cotton fibers, straight nylon fiber with high abrasion resistance is the most widely used flocking fiber [46, 47] (Figure S6); therefore, nylon fiber is selected for further investigation. Besides, the microstructure of the fiber array is regulated by controlling the length of nylon fiber, flocking voltage, and flocking time, thereby optimizing the liquid absorption time. Compared with long nylon fiber (300.3–661.3 μm, 71.7°), only more hydrophobic short nylon fiber (205.7 μm, 83.9°) is available (Figures S7 and S8). Therefore, the impact of shorter fiber on the liquid absorption performance of MA-PA-FS remains unclear at present (Figure 2b). It takes approximately 10 ms for a 5 μL water droplet to be absorbed completely into the MA-PA-FS with a fiber length larger than 300.3 μm (Figure 2b). Thus, samples

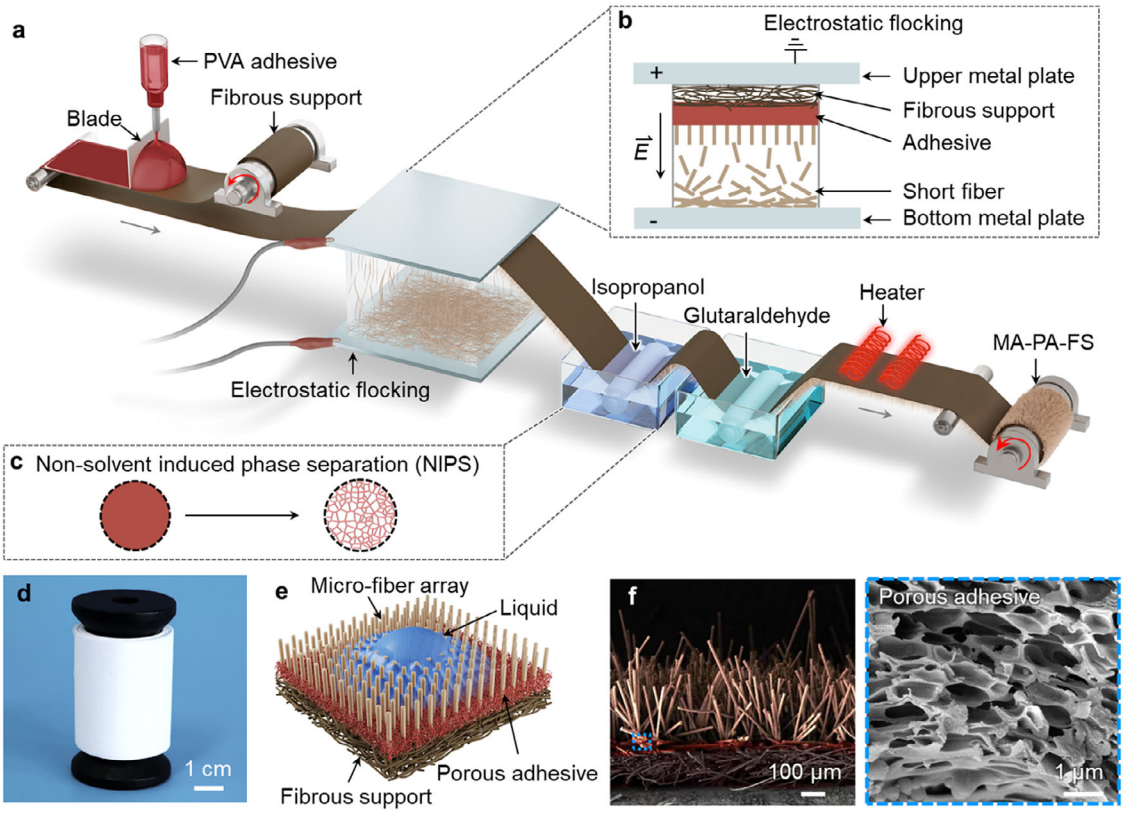

FIGURE 1 | Semi-continuous fabrication and structural characterization of the trilayer MA-PA-FS composite. (a) Schematic representation of the fabrication process: blade coating of PVA solution onto a non-woven fabric, electrostatic flocking of microfibers, immersion in isopropanol to induce phase separation and porosity, cross-linking with glutaraldehyde, followed by drying and collection. (b) Mechanism of electrostatic flocking for aligned microfiber attachment. (c) Schematic representation of non-solvent-induced phase separation for creating a porous adhesive layer. (d) Photograph of a semi-continuously produced MA-PA-FS roll (4 cm width). (e) Structural model depicting the three layers of the MA-PA-FS composite and ultrafast liquid absorption enabled by the integration of lateral spreading and vertical imbibition. (f) Cross-sectional SEM images showing vertically aligned microfiber anchored via the porous PVA adhesive interlayer.

with different thicknesses can be obtained by adjusting the length of the nylon fiber. In this work, a 300.3 μm nylon fiber is selected for further investigation. Flocking time and voltage have limited impact on the density of the micro-fiber array (Figures S9 and S10), resulting in fast liquid absorption regardless of flocking time and voltage. The optimized fiber length, flocking voltage, and flocking time are 300.3 μm, 12 kV, and 60 s (Figure 2b).

As an important component of the MA-PA-FS, porous PVA not only serves as adhesive but also as a liquid transport channel; therefore, the microstructure of the porous PVA adhesive layer is regulated via different PVA concentrations and phase separation times. As shown in Figure S11, pore size increases with increasing PVA concentration. The viscosity of the 5% PVA solution is too low to stick the micro-fiber firmly, while a high concentration of 15% leads to decreased connectivity of the porous PVA adhesive interlayer, which is conducive to liquid absorption. Correspondingly, MA-PA-FS prepared with 10% PVA solution shows the shortest liquid absorption time (Figure 2c). The PVA adhesive interlayer exhibits a smaller and more homogeneous pore structure with longer phase separation time in isopropanol (Figure S12), leading to shorter liquid absorption time. Considering both experimental efficiency and liquid absorption performance, a phase separation time of 180 min is selected for further investigation (Figure 2c). Apart from the micro-fiber array and porous adhesive interlayer, varied fibrous supports are used to prepare the MA-PA-FS. As shown in Figure 2d and Figures S13 and S14, despite the varying wettability of different fibrous supports, the liquid absorption times on MA-PA-FS prepared with different fibrous supports are less than 20 ms, indicating that the influence of the wettability of the fibrous support on the absorption time of MA-PA-FS is limited. Fibrous supports such as cellulose acetate (CA) membrane and nonwoven fabric with more uniform microstructure result in a regularly arranged micro-fiber array, leading to shorter liquid absorption time. These results also indicate the broad substrate compatibility of this method. The average height (h), width (w), and distance (d) of the micro-fiber array of the optimized MA-PA-FS are 300.3 ± 11.4, 9.8 ± 1.3, and 24.1 ± 7.5 μm, respectively (Figure 2e). The liquid absorption time across an MA-PA-FS roll sample with a size of 4 × 10 cm is below 14 ms, confirming high uniformity in both length and width directions (Figure S15).

2.3 | Water Absorption Dynamics

Figure 3 presents the absorption dynamics of a water droplet on different composite structures. As shown in Figure 3a,b, and Figures S16a and S17, and Movie S4, when a water droplet is placed gently on the front surface of MA-PA-FS, the droplet rapidly spreads out into two parts: the bulk and the fringe.

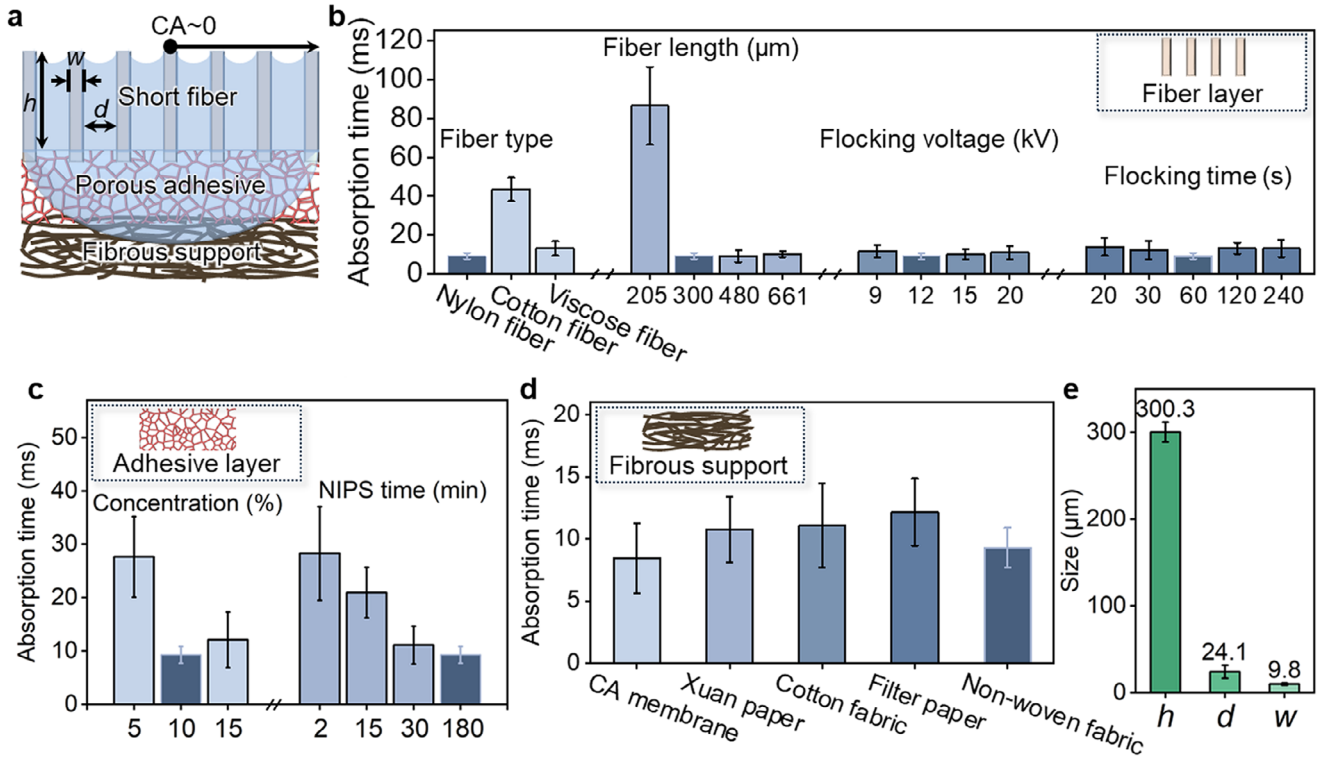

FIGURE 2 | Optimization of fabrication parameters for the MA-PA-FS composite. (a) Schematic representation of liquid absorption measurement and the corresponding microstructure of the composite. (b) Absorption time as a function of fiber layer parameters: fiber type, length, flocking voltage, and flocking time. (c) Absorption time versus PVA concentration and phase-separation duration. The fastest absorption is achieved at 10% PVA and 180 min phase separation. (d) Absorption time for MA-PA-FS prepared with different fibrous supports. All absorption tests are performed with a 5 μL water droplet. (e) Statistical distributions of the micro-fiber array dimensions: height (h), width (w), and inter-fiber distance (d). ($n = 5$).

The water droplet promptly expands initially, with the fringe propagating faster than the bulk. Subsequently, the bulk ceases to expand and starts to contract over time as it acts as a reservoir to maintain the propagation of the fringe film, as evidenced in Figure 3b and Figure S17. In contrast, different absorption dynamics are observed on the rear side of the MA-PA-FS. A water droplet with the same volume imbibes into the rear side at 480.0 s (Figure 3d,e,g and Movie S5), which is four orders of magnitude longer than that on the front (9.3 ms). Compared with the front side, the solely vertical imbibition and diminished base radius on the rear side result in longer liquid absorption time (Figure 3g and Figure S18). Unidirectional liquid transport, also known as the liquid-diode effect, allows liquid to flow in one direction while blocking its backflow. Here, we monitored different volumes of water transport through the MA-PA-FS from both the front (micro-fiber array layer) and the rear side (fibrous support layer). As shown in Figure 3c, 0.2 and 5 μL water droplets (dyed pink to aid observation) can easily penetrate the MA-PA-FS from the front to the rear side, while being blocked from penetrating in the opposite direction. However, as shown in Figure 3f, for the liquid applied onto the rear side, there is only slight penetration to the front side until the liquid volume is increased to 40 μL. Therefore, the threshold for liquid permeation in both cases differs significantly: less than 0.2 μL from the front side versus 40 μL from the rear side. The contrasting liquid penetration behaviors on the two opposite sides demonstrate the unidirectional water absorption of the MA-PA-FS. Compared to MA-PA-FS, the counterpart micro-fiber array-dense adhesive interlayer-fibrous support (MA-DA-FS) is a sample featuring micro-fiber array clinging to non-woven fabric via dense PVA adhesive interlayer (Figure S19); the porous adhesive interlayer-fibrous support (PA-FS) is a sample with solely porous PVA layer on non-woven fabric (Figure S20). The absorption times of a 5 μL droplet on MA-DA-FS and PA-FS are 517.6 and 90,000 ms, respectively (Figure 3h and Figures S21 and S22). The experimental liquid absorption time for a 5 μL droplet on MA-PA-FS (9.3 ms) is three orders of magnitude smaller than that on the PA-FS (90,000 ms), which is comparable to the theoretically calculated value (~2.3×10^3, Note S1). Considering the same hydrophilic compounds of MA-PA-FS, MA-DA-FS, and PA-FS, different absorption dynamics on these three samples mainly originated from structural differences. As uncovered in our previous work [27], the structural feature of MA-PA-FS results in simultaneous lateral liquid spreading and vertical imbibition of liquid, facilitating the ultrafast absorption of liquid upon an augmented base radius. Therefore, the combination of flocking and NIPS is necessary to achieve ultrafast, unidirectional liquid absorption. Moreover, the absorption times on MA-PA-FS for droplets with volumes of 1, 5, and 10 μL are 6.5, 9.3, and 13.9 ms, respectively (Figure 3i and Figures S23 and S24), indicating that liquid droplets can be absorbed in milliseconds. The MA-PA-FS composite demonstrates a short absorption time of 9.3 ms for a 5 μL fluorescent water droplet (liquid absorption rate: 537.6 μL s^{-1}), far beyond that of the previously reported porous substrate with unidirectional liquid transport (less than 50 μL s^{-1}) (Figure S25).

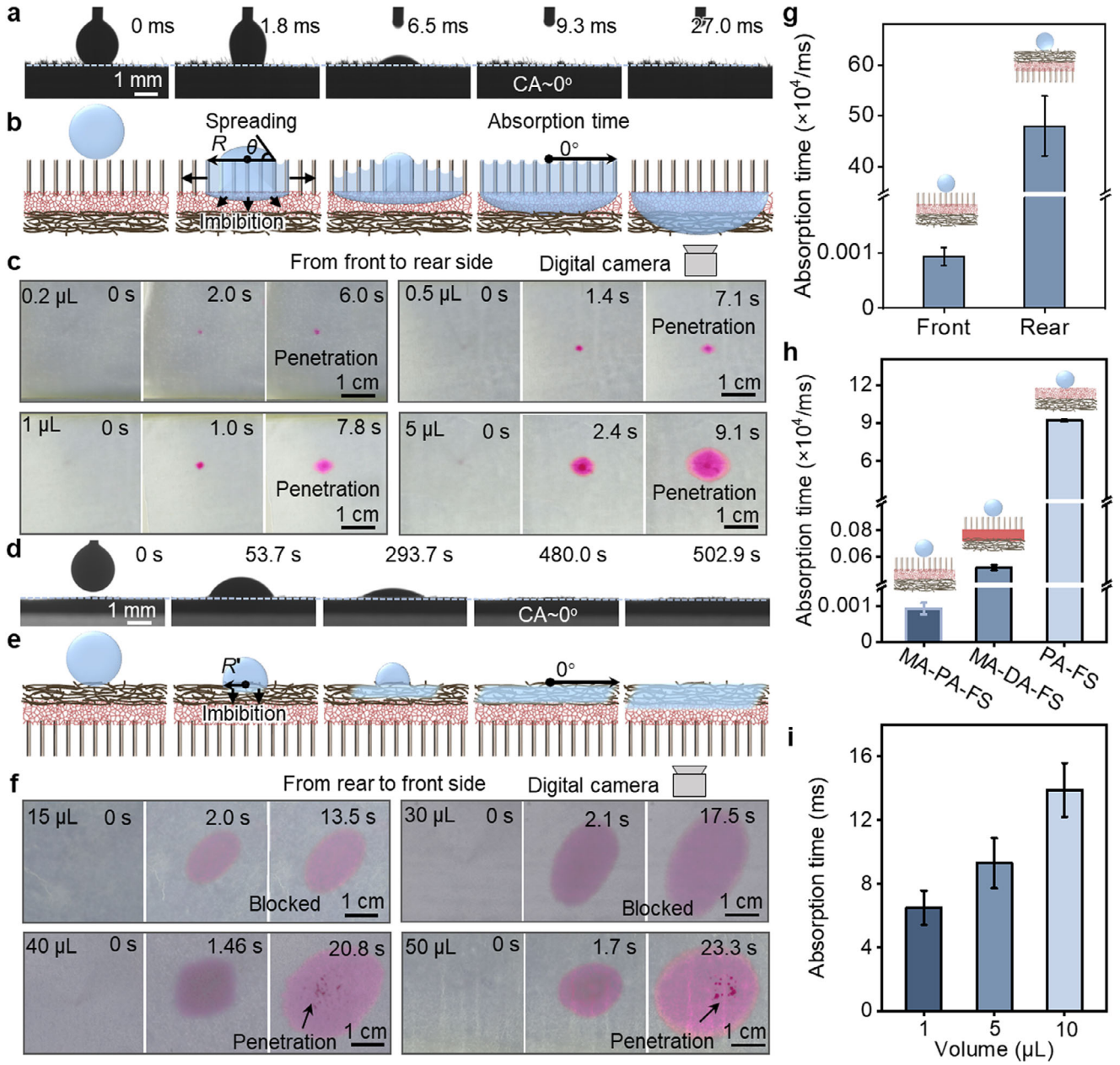

FIGURE 3 | Water absorption dynamics of composite structures. (a,d) Time-lapse images and (b,e) corresponding schematics of a 5 μL dyed water droplet (1% fluorescein disodium salt) spreading and imbibing into the (a,b) front side and (d,e) rear side of the MA-PA-FS. The droplet is fully absorbed in 9.3 ms (front) versus 480.0 s (rear). (c,f) Unidirectional water transport within the MA-PA-FS. Water transport performance from (c) the front side (micro-fiber array layer) to the rear side (fibrous support) and (f) from the rear side to the front side. (g) Statistics of water absorption time from the front and rear sides of the MA-PA-FS composite. (h) Absorption time of different composite structures. MA-PA-FS, which combines micro-fiber array and porous adhesive interlayer, shows the shortest absorption time. (i) Absorption times on the front side of the MA-PA-FS for droplets with volumes of 1, 5, and 10 μL. ($n = 5$).

2.4 | Viscous Liquid Absorption, Moisture Permeability and Abrasion Resistance

Biofluids that need to be rapidly removed from the body surface typically possess high viscosity. Thus, we explore the absorption dynamics of viscous liquid on MA-PA-FS. As shown in Figure S26, PVA solution with increasing concentration shows increased viscosity (1.0–50.9 mPa s) and decreased surface tension (72.3–44.7 mN m^{-1}). With the increase in liquid viscosity, the viscous resistance within the porous structure increases, leading to longer liquid absorption time (Figure 4a). The overall absorption time for a highly viscous PVA solution with 8.0% concentration and viscosity of 50.9 mPa s is less than 190 ms, indicating its ultrafast absorption even for viscous liquid. To evaluate real biofluid absorption dynamics, porcine blood with a viscosity of 4.1 mPa s and a surface tension of 61.4 mN m^{-1} is used (Figure S27), and the results are shown in Figure 4b and Movie S6. Porcine blood is absorbed completely into MA-PA-FS, while a lot of blood

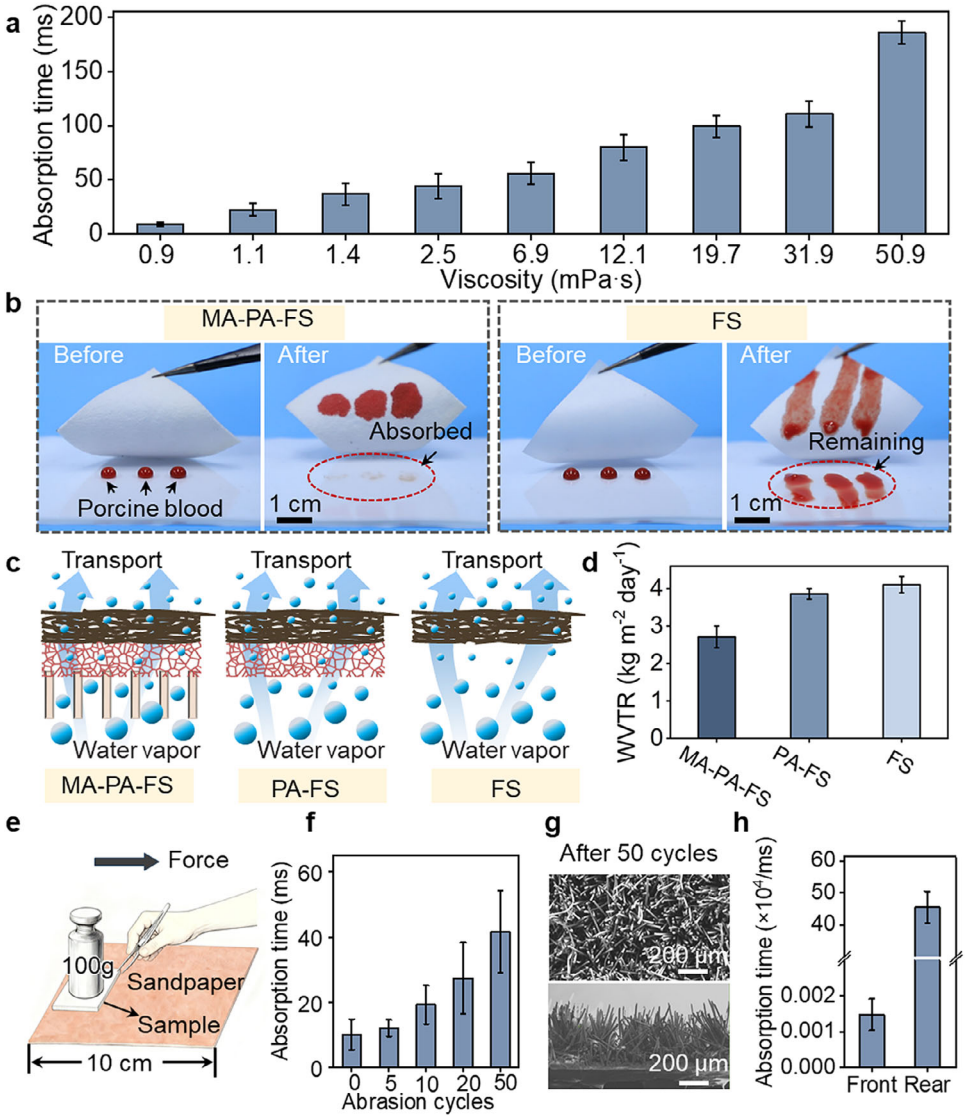

FIGURE 4 | Viscous liquid absorption, moisture permeability and abrasion resistance of the MA-PA-FS composite. (a) Liquid absorption time as a function of viscosity ($n = 5$). (b) Absorption of fresh porcine blood by MA-PA-FS, compared with the fibrous support (FS, solely nonwoven fabric). (c) Schematic representation of moisture transport through the MA-PA-FS, PA-FS, and FS structure. (d) The MA-PA-FS shows a water vapor transmission rate (WVTR) of 2.7 kg m^{-2} day^{-1}, indicating high moisture permeability ($n = 3$). (e) Schematic diagram of sandpaper abrasion test. (f) Liquid absorption time ($n = 3$) and (g) microstructure of the MA-PA-FS after continuous abrasion cycles of 50. (h) Liquid absorption time on the front and rear side of MA-PA-FS after 100 cycles of bending-compression ($n = 3$).

is left after being absorbed by FS. The MA-PA-FS with efficient absorption capability of viscous biofluid shows great potential as a wound dressing.

Apart from liquid absorption property, good moisture permeability is essential for maintaining comfort under many practical conditions. WVTR of different samples is tested by the water vapor transmission cup method (Figure S28). As shown in Figure 4c,d, the MA-PA-FS, PA-FS, and FS present WVTR of 2.71, 3.86, and 4.11 kg m^{-2} day^{-1}, respectively. Compared to FS, the presence of a porous adhesive layer and micro-fiber array reduces water vapor permeability. However, it is impressive that the MA-PA-FS retains an interconnected pore structure along the vertical axis of the sample, ensuring good water vapor permeability (Figure 4c), which is comparable to cotton fabric [48, 49]. It is noteworthy that the bonding strength of micro-fiber to the fibrous support is particularly important for the practical application of the MA-PA-FS. Herein, the mechanical durability of MA-PA-FS is evaluated through a sandpaper abrasion test (Figure 4e). According to the results in Figure 4f, the liquid absorption time for a 5 μL droplet on MA-PA-FS is less than 45 ms after 50 cycles of abrasion. After the abrasion test, an SEM image of the MA-PA-FS is measured and shown in Figure 4g; the micro-fiber array is still anchored perpendicular to the non-woven fabric, indicating the high robustness of the MA-PA-FS. In addition, the liquid absorption times for a 5 μL droplet on the front and rear sides of MA-PA-FS are 14.8 and 455 000 ms, respectively, after 100 cycles of bending-compression (Figure 4h and Figure S29), indicating that unidirectional liquid absorption performance is well maintained after mechanical disturbance. The MA-PA-FS demonstrates ultrafast, unidirectional liquid absorption, good water vapor permeability, and high robustness.

3 | Conclusions

In conclusion, unlike conventional microfabrication approaches, we present a scalable in-line manufacturing strategy that integrates electrostatic flocking with sequential non-solvent-induced phase separation and cross-linking, enabling semi-continuous fabrication of microfiber-covered porous composites. The resulting trilayer architecture—composed of a vertically aligned microfiber array, porous PVA adhesive interlayer, and a fibrous support—exhibits engineered synergy between lateral capillary spreading and vertical imbibition. Through systematic optimization of each structural component, the composite achieves ultrafast unidirectional liquid absorption, absorbing a 5 μL water droplet within 9.3 ms, which outperforms conventional porous surfaces by three orders of magnitude, and maintains rapid absorption even for viscous biofluids. Coupled with high moisture permeability and robust mechanical durability, this composite structure holds great potential for further functional modification, including antibacterial, conductive, and infrared-shielding properties, to fabricate next-generation functional textiles, wearable devices, and advanced wound care materials. Our work establishes a scalable pathway toward high-performance liquid-management interfaces for practical biomedical and protective applications.

4 | Materials and Methods

4.1 | Materials

Poly(vinyl alcohol) (PVA) with weight-average molecular weight (M_w) of ~ 205 000 was purchased from Shanghai Macklin Biochemical Co., Ltd. Glutaraldehyde (50%) was obtained from Beijing Innochem Science & Technology Co., Ltd. Isopropanol (AR) was supplied by Tianjin FuYu Fine Chemical Co., Ltd. Hydrochloric acid (36.0%–38.0%) was acquired from Luoyang Haohua Chemical Reagent Co., Ltd. Fluorescein disodium salt (AR) was purchased from J&K Scientific Ltd. (Beijing, China). Nylon, viscose, and cotton short fiber were purchased from Hongxin Printing Factory, located in Zhongshan, Guangdong Province, China. Nylon fibers with lengths of 300.3, 480.7, and 661.3 μm are white. Black nylon fiber with a length of 205.7 μm was purchased due to the lack of white short nylon fiber. Non-woven fabric with a thickness of 93.2 ± 2.6 μm was purchased from Anhui Qinglan New Material Technology Co., Ltd. Cotton fabric with a thickness of 160.0 ± 5.1 μm was supplied by Hongda Textile Factory located in Shijiazhuang, Hebei Province, China. Cellulose acetate membrane (CA membrane, pore size: 0.8 μm) with a thickness of 133.7 ± 2.5 μm was purchased from Shanghai Xinya Purification Equipment Co., Ltd., Shanghai, China. Filter paper with a thickness of 165.0 ± 3.7 μm was purchased from Shanghai Titan Technology Co., Ltd., China. Xuan paper with a thickness of 132.5 ± 5.5 μm was purchased from Yubaoge located in Xuancheng, Anhui Province, China. Fibrous support thickness is presented as mean ± standard deviation (n = 3 independent measurements for our experimental group).

4.2 | Fabrication of MA-PA-FS

PVA solutions with concentrations of 5, 10, and 15 wt% were prepared by dissolving PVA into deionized water after stirring at 90°C for 1 h. Subsequently, the PVA solution was blade-coated on the moving non-woven fabric (final winding speed: 27 cm min^{-1}) using an adjustable film applicator KTQ-III with a gap size of 300 μm. In the electrostatic flocking process, as shown in Figure 1a and Figure S3, the PVA-coated side was subjected to flocking, and a potential of 9–20 kV was applied between the two electrodes. The electrostatic high voltage generator (RS485) was purchased from Qingdao Pansi Technology Co., Ltd. The upper and lower electrode plates were aluminum plates (200 × 140 × 0.8 mm), and the distance between the upper and lower electrode plates was 10 cm. Short fibers were charged and propelled from the bottom plate to the top one due to electrostatic attraction. These short fibers were stuck to non-woven fabric by the PVA solution. During this process, the short fibers tended to align along the electric field direction, and finally numerous short fibers were oriented vertically on the surface. The flocking time was 20–240 s. Next, the flocked fabric was immersed in isopropanol for 2–180 min to induce phase separation, followed by crosslinking in a glutaraldehyde solution (3.3 wt%, pH = 3) for 30 min. Then the sample was dried at 60°C for 30 min under an infrared heater (wavelength: 6–12 μm) to provide a roll of MA-PA-FS. The distance between the infrared heat source and the sample is 2.4 cm, and the temperature of the infrared heat source can be regulated by the power adjustment knob on the device. Generally, nylon fibers and non-woven fabrics are widely used in biomedical applications [50]. However, for biomedical applications, the removal of glutaraldehyde and unreacted aldehyde groups in the porous adhesive interlayer via post-treatment is necessary to improve biocompatibility [51, 52].

By replacing the isopropanol immersion (phase separation process) with heating at 60°C for 3 h, a micro-fiber array-dense adhesive interlayer-fibrous support (MA-DA-FS) was prepared. PVA solution-coated non-woven fabric without micro-fiber array was immersed in isopropanol to prepare porous adhesive interlayer-fibrous support (PA-FS).

4.3 | Characterization

The microstructure of the sample was examined using a field emission scanning electron microscope (SEM, JSM-7900F, JEOL), with samples subjected to Au sputtering (E-1045, Hitachi) with 20 mA current for 120 s before observation. A cross-section of the sample was prepared by cryogenic fracture using liquid nitrogen. Specifically, a notch of ~2 mm depth was created at the edge of the sample using a double-edged blade, and the notched sample was immersed in liquid nitrogen for 30 s. Then, the sample was removed from the liquid nitrogen and immediately snapped at the notch using two pairs of tweezers. A relatively clean cross-section was obtained for SEM observation. Porosity of the porous PVA adhesive layer was quantified utilizing nitrogen adsorption analyses (BELSORP-max II, BEL, Japan). Water contact angle (WCA) was measured using a contact angle measurement system (OSA100, LAUDA, Germany) with a 3 μL water droplet at room temperature. The WCA was determined by Young-Laplace fitting and averaged from five points on each sample. The viscosities of different solutions were tested on a rheometer (DHR2, TA Instruments, U.S.A), using a parallel plate (20 mm in diameter) method with a gap of 0.25 mm and a shear rate of 300 s^{-1} at

25°C. The surface tensions of different solutions were measured using the pendant drop volume method on a contact angle measurement system (OSA100, LAUDA, Germany), and five individual measurements were taken for each solution.

4.4 | Dynamic Liquid Absorption Behavior

To facilitate observation, water droplets used in the whole manuscript were dyed with 1% fluorescein disodium salt. The deionized water (DI) dyed with 1% fluorescein disodium salt shows a surface tension of 70.2 mN m^{-1} and a viscosity of 1.03 mPa·s (20°C). A water droplet was precisely placed onto the surface of the substrate using a pipette. The dynamic spreading and imbibition of the droplet were concurrently captured from overhead with a high-speed camera (PHANTOM VEO E 310L, Phantom, America, 1000 fps) and laterally with a contact angle measurement system (OSA100, LAUDA, Germany, 1000 fps). In addition, upon application of a 1 µL water droplet dyed with 1% fluorescein disodium salt, the advancements of both the fringe film and the bulk phase were monitored using a combination of an optical microscope (Axioscope 5, Zeiss, Oberkochen, Germany) and a high-speed camera (1000 fps). Absorption behaviors of viscous liquid and porcine blood on MA-PA-FS were tested using a contact angle measurement system (1000 fps).

4.5 | Unidirectional Liquid Absorption Performance

To determine the unidirectional liquid absorption performance, rhodamine B-dyed water droplets with different volumes were deposited on the front and rear sides of the MA-PA-FS. The permeation of liquid on the opposite side of the sample was recorded by a digital camera (Canon 100 mm F2.8L IS USM, Japan) until the absorption was completed.

4.6 | Moisture Permeability and Mechanical Durability

To determine the moisture permeability, WVTR of the non-woven fabric, MA-PA-FS, and PA-FS was tested. 80 g of deionized water was filled into the clean glass vial, and the vial was sealed with different samples. The gap between the sample and the glass vial rim was first sealed using double-sided tape, and the outer edge was further sealed with glue and plastic wrap. Then, the vial was placed in an environmental test chamber (AH-80A, Guangdong Atmars Test Equipment Co., Ltd.) to maintain the temperature at 38°C and the relative humidity at 65%. The vial was weighed after 24 h, and the WVTR was calculated according to the reduced weight (Figure S28).

For the abrasion resistance test, a sandpaper (2000 mesh) was used as an abrasion surface. The MA-PA-FS bearing a load of 100 g was placed on the sandpaper and moved for a distance of 10 cm (linear abrasion for 10 cm and then go back to the starting point) as 1 cycle. Liquid absorption time and microstructure were monitored to evaluate the mechanical durability of the MA-PA-FS.

Cyclic bending test was carried out on an Instron universal testing machine (Instron 5965, Instron Inc., USA). A sample strip (1 × 2 cm) was adhered at both ends to the compression stage and subjected to 100 bending-compression cycles under a 1 N load (Figure S29). Liquid absorption times on the front and rear sides were tested.

Author Contributions

Jie Ju, Yu-Qiong Luo, and Xi Yao conceived and designed the work; Yonghua Li fabricated MA-PA-FS and conducted water absorption, moisture permeability, and abrasion resistance experiments; Yu-Qiong Luo and Yonghua Li. analyzed related data; Ming Li, Ximeng Zhang, and Tianzhi Li created a schematic diagram, Yu-Qiong Luo drafted the original manuscript. Jie Ju, Xi Yao, and Lei Jiang edited the manuscript.

Acknowledgements

This work was financially supported by the National Natural Science Foundation of China (52573111, 22472047 and U23A20122) to Luo Y.-Q., Ju J., and Yao X., Natural Science Foundation of Henan Province (252300423106 and 262300421178) to Luo Y.-Q. and Ju J. The Joint funds from Longzihu New Energy Laboratory are greatly appreciated.

Conflicts of Interest

One patent for biomimetic ultrafast permeation surface and its preparation, with filing number 202510446852.1, has been filed by Henan University.

Data Availability Statement

All data are available in the main text or the Supporting Information.

References

1. F. Feng, Z. Zhao, J. Li, Y. Huang, and W. Chen, "Multifunctional Dressings for Wound Exudate Management," *Progress in Materials Science* 146 (2024): 101328, https://doi.org/10.1016/j.pmatsci.2024.101328.

2. W. Berry, J. Bonville, and S. D. Blatt, "Diaper Need — An Underrecognized Social Driver of Health," *New England Journal of Medicine* 393 (2025): 939–940, https://doi.org/10.1056/NEJMp2506744.

3. B. Zhang, J. Li, J. Zhou, et al., "A Three-Dimensional Liquid Diode for Soft, Integrated Permeable Electronics," *Nature* 628 (2024): 84–92, https://doi.org/10.1038/s41586-024-07161-1.

4. S. Kim, S. Park, J. Choi, et al., "An Epifluidic Electronic Patch With Spiking Sweat Clearance for Event-Driven Perspiration Monitoring," *Nature Communications* 13 (2022): 6705, https://doi.org/10.1038/s41467-022-34442-y.

5. Y. Zhang, J. Fu, Y. Ding, et al., "Thermal and Moisture Managing E-Textiles Enabled by Janus Hierarchical Gradient Honeycombs," *Advanced Materials* 36 (2024): 2311633, https://doi.org/10.1002/adma.202311633.

6. X. Kuang, Z. Zhang, H. He, et al., "Biomimetic Janus Membrane With Spongy Channels for Directional Liquid Transport," *Nature Communications* 16 (2025): 10001, https://doi.org/10.1038/s41467-025-64964-0.

7. C. Shi, H. Wang, X. Wang, et al., "A Safe, Stable, Simple, Serviceable, and Self-Powered Wound Dressing With Continuous Low-Voltage Direct Current Electrical Stimulation: An Efficient Approach to Accelerate Wound Healing," *Advanced Functional Materials* 35 (2025): 2422188, https://doi.org/10.1002/adfm.202422188.

8. L. Liu, H. Sun, J. Zhang, et al., "Trilayered Fibrous Dressing With Wettability Gradient for Spontaneous and Directional Transport of Massive

Exudate and Wound Healing Promotion," *Advanced Fiber Materials* 5 (2023): 574–587, https://doi.org/10.1007/s42765-022-00239-3.

9. L. Wang, Y. Luo, Y. Song, X. He, T. Xu, and X. Zhang, "Hydrogel-Functionalized Bandages With Janus Wettability for Efficient Unidirectional Drug Delivery and Wound Care," *ACS Nano* 18 (2024): 3468–3479, https://doi.org/10.1021/acsnano.3c10766.

10. U. Sen, S. Chatterjee, P. Sinha Mahapatra, et al., "Surface-Wettability Patterning for Distributing High-Momentum Water Jets on Porous Polymeric Substrates," *ACS Applied Materials & Interfaces* 10 (2018): 5038–5049, https://doi.org/10.1021/acsami.7b13744.

11. M. Hashmi, S. Ullah, A. Ullah, et al., "An Optimistic Approach "From Hydrophobic to Super Hydrophilic Nanofibers" for Enhanced Absorption Properties," *Polymer Testing* 90 (2020): 106683, https://doi.org/10.1016/j.polymertesting.2020.106683.

12. X. Chen, H. Guo, Y. Feng, et al., "Full Micro-Nanofiber Aerogel With Three-Dimensional Fluffy Network Structure for Rapid Liquid Absorption and Uniform Liquid Retention in Diapers," *Materials Today Chemistry* 40 (2024): 102191, https://doi.org/10.1016/j.mtchem.2024.102191.

13. Y. Zheng, H. Bai, Z. Huang, et al., "Directional Water Collection on Wetted Spider Silk," *Nature* 463 (2010): 640–643, https://doi.org/10.1038/nature08729.

14. J. Ju, H. Bai, Y. Zheng, T. Zhao, R. Fang, and L. Jiang, "A Multi-Structural and Multi-Functional Integrated Fog Collection System in Cactus," *Nature Communications* 3 (2012): 1247, https://doi.org/10.1038/ncomms2253.

15. M. Prakash, D. Quéré, and J. W. M. Bush, "Surface Tension Transport of Prey by Feeding Shorebirds: The Capillary Ratchet," *Science* 320 (2008): 931–934, https://doi.org, 10.1126/science.1156023.

16. A. R. Parker and C. R. Lawrence, "Water Capture by a Desert Beetle," *Nature* 414 (2001): 33–34, https://doi.org/10.1038/35102108.

17. S. Feng, P. Zhu, H. Zheng, et al., "Three-Dimensional Capillary Ratchet-Induced Liquid Directional Steering," *Science* 373 (2021): 1344–1348, https://doi.org, 10.1126/science.abg7552.

18. S. Kumar, A. Borbora, P. Chakraborty, et al., "Controlled Chemical-Patterning of Textile to Accelerate Anti-Gravity Water Flow," *Advanced Functional Materials* 34 (2024): 2410955, https://doi.org/10.1002/adfm.202410955.

19. L. Lao, D. Shou, Y. S. Wu, and J. T. Fan, "Skin-Like" Fabric for Personal Moisture Management," *Science Advances* 6 (2020): aaz0013, https://doi.org/10.1126/sciadv.aaz0013.

20. Q. Zhang, Y. Li, Y. Yan, X. Zhang, D. Tian, and L. Jiang, "Highly Flexible Monolayered Porous Membrane With Superhydrophilicity–Hydrophilicity for Unidirectional Liquid Penetration," *ACS Nano* 14 (2020): 7287–7296, https://doi.org/10.1021/acsnano.0c02558.

21. K. Li, H. Li, Y. Xue, H. Yang, C. Zhang, and Z. Xu, "Photothermal Janus Fabrics Enabling Persistent Directional Sweat-Wicking in Personal Wet-Thermal Management," *Journal of Colloid and Interface Science* 651 (2023): 841–848, https://doi.org/10.1016/j.jcis.2023.08.044.

22. Y. Peng and Y. Cui, "Advanced Textiles for Personal Thermal Management and Energy," *Joule* 4 (2020): 724–742, https://doi.org/10.1016/j.joule.2020.02.011.

23. W. Xiao, X. Wan, L. Shi, M. Ye, Y. Zhang, and S. Wang, "A Viscous-Biofluid Self-Pumping Organohydrogel Dressing to Accelerate Diabetic Wound Healing," *Advanced Materials* 36 (2024): 2401539, https://doi.org/10.1002/adma.202401539.

24. H. R. Charles-Williams, R. Wengeler, K. Flore, H. Feise, M. J. Hounslow, and A. D. Salman, "Granule Nucleation and Growth: Competing Drop Spreading and Infiltration Processes," *Powder Technology* 206 (2011): 63–71, https://doi.org/10.1016/j.powtec.2010.06.013.

25. A. Clarke, T. D. Blake, K. Carruthers, and A. Woodward, "Spreading and Imbibition of Liquid Droplets on Porous Surfaces," *Langmuir* 18 (2002): 2980–2984, https://doi.org/10.1021/la0117810.

26. S. Krainer and U. Hirn, "Contact Angle Measurement on Porous Substrates: Effect of Liquid Absorption and Drop Size," *Colloids and Surfaces A: Physicochemical and Engineering Aspects* 619 (2021): 126503, https://doi.org/10.1016/j.colsurfa.2021.126503.

27. Y. Wang, L. Zhao, Y.-Q. Luo, et al., "Ultra-Fast, Unidirectional Water Absorption on Wood Ear," *Advanced Materials* 37 (2025): 2413364, https://doi.org/10.1002/adma.202413364.

28. A. McCarthy, J. V. John, L. Saldana, et al., "Electrostatic Flocking of Insulative and Biodegradable Polymer Microfibers for Biomedical Applications," *Advanced Healthcare Materials* 10 (2021): 2100766, https://doi.org/10.1002/adhm.202100766.

29. M. Shen, S. Deng, H. Pi, et al., "Electrostatic Flocking: Reborn to Embrace Multifunctional Applications," *Small Structures* 6 (2025): 2500143, https://doi.org/10.1002/sstr.202500143.

30. X. Chen, Y. Gu, J. Liang, et al., "Enhanced Microwave Shielding Effectiveness and Suppressed Reflection of Chopped Carbon fiber Felt by Electrostatic Flocking of Carbon fiber," *Composites Part A: Applied Science and Manufacturing* 139 (2020): 106099, https://doi.org/10.1016/j.compositesa.2020.106099.

31. Z. Wu, Y. Zhao, Y. Duo, et al., "Silk Flocked Flexible Sensor Capable of Wide-Range and Sensitive Pressure Perception," *ACS Applied Materials & Interfaces* 16 (2024): 64222–64232, https://doi.org/10.1021/acsami.4c13315.

32. P. Lyu, W. Shi, Y. Liu, et al., "Adaptable, Dynamic, and Superhydrophobic Standing-Fiber Surface With Muti-Level Energy Barrier for Anti-Icing," *Advanced Functional Materials* 35 (2025): 2421174, https://doi.org/10.1002/adfm.202421174.

33. G. Liu, J. Yang, K. Zhang, et al., "Recent Progress on the Development of Bioinspired Surfaces With High Aspect Ratio Microarray Structures: From Fabrication to Applications," *Journal of Controlled Release* 367 (2024): 441–469, https://doi.org/10.1016/j.jconrel.2024.01.054.

34. M. Kim, S. Yoo, H. E. Jeong, and M. K. Kwak, "Fabrication of Salvinia-Inspired Surfaces for Hydrodynamic Drag Reduction by Capillary-Force-Induced Clustering," *Nature Communications* 13 (2022): 5181, https://doi.org/10.1038/s41467-022-32919-4.

35. S. He, Y. Tian, H. Zhou, et al., "Review for Micro-Nano Processing Technology of Microstructures and Metadevices," *Advanced Functional Materials* 35 (2025): 2420369, https://doi.org/10.1002/adfm.202420369.

36. F. Mayer, S. Richter, J. Westhauser, E. Blasco, C. Barner-Kowollik, and M. Wegener, "Multimaterial 3D Laser Microprinting Using an Integrated Microfluidic System," *Science Advances* 5 (2019): aau9160, https://doi.org/10.1126/sciadv.aau9160.

37. L. Liu, X. Y. Gao, S. S. Zheng, X. Yao, J. Ju, and L. Jiang, "Recent Progress on Liquid Superspreading and Its Applications," *Advanced Materials* 37 (2025): 2501734, https://doi.org/10.1002/adma.202501734.

38. X. Sun, G. Sun, and X. Wang, "Morphology Modeling for Polymer Monolith Obtained by Non-Solvent-Induced Phase Separation," *Polymer* 108 (2017): 432–441, https://doi.org/10.1016/j.polymer.2016.12.026.

39. S. J. Bohr, F. Wang, M. Metze, et al., "State-Of-The-Art Review of Porous Polymer Membrane Formation Characterization—How Numerical and Experimental Approaches Dovetail to Drive Innovation," *Frontiers in Sustainability* 4 (2023): 1–28, https://doi.org/10.3389/frsus.2023.1093911.

40. X. Tan and D. Rodrigue, "A Review on Porous Polymeric Membrane Preparation. Part I: Production Techniques With Polysulfone and Poly (Vinylidene Fluoride)," *Polymers* 11 (2019): 1160, https://doi.org/10.3390/polym11071160.

41. N. Sun, S. Mo, Y. Cai, et al., "Bicontinuous Porous Substrates by Polysulfone/2-pyrrolidone Binary System for High-Performance Forward Osmosis Membranes," *Journal of Membrane Science* 717 (2025): 123614, https://doi.org/10.1016/j.memsci.2024.123614.

42. Y. Xu, Z. Ye, G. Zhao, et al., "Phase-Separated Porous Nanocomposite With Ultralow Percolation Threshold for Wireless Bioelectronics," *Nature*

Nanotechnology 19 (2024): 1158–1167, https://doi.org/10.1038/s41565-024-01658-6.

43. W. Peng, Y. Cao, S. Lin, and T. Wu, "Development of Porous Nitrocellulose Membrane for Lateral Flow Immunoassays," *Journal of Membrane Science* 735 (2025): 124591, https://doi.org/10.1016/j.memsci.2025.124591.

44. A. A. Sapalidis, "Porous Polyvinyl Alcohol Membranes: Preparation Methods and Applications," *Symmetry* 12 (2020): 960, https://doi.org/10.3390/sym12060960.

45. S. K. Chae, C. H. Mun, D. Y. Noh, E. Kong, and S. H. Lee, "Simple Fabrication Method for a Porous Poly(vinyl alcohol) Matrix by Multisolvent Mixtures for an Air-Exposed Model of the Lung Epithelial System," *Langmuir* 30 (2014): 12107–12113, https://doi.org/10.1021/la501453h.

46. S. W. Bolgen, "Flocking Technology," *Journal of Industrial Textiles* 21 (1991): 123–131, https://doi.org/10.1177/152808379102100206.

47. R. L. Coldwell and S. P. Hersh, "The Influence of Processing Variables on the Properties of Flocked Fabrics," *IEEE Transactions on Industry Applications* IA-14 (1978): 175–182, https://doi.org/10.1109/TIA.1978.4503514.

48. S. Bi, Y. Yang, G. Pei, T. Yang, S. Hu, and Q. Jia, "Unidirectional Moisture-Conducting Green Fabrics Prepared by a One-Step Electrospray Technique," *RSC Advances* 15 (2025): 1125–1133, https://doi.org/10.1039/d4ra08289c.

49. S. Mondal and J. L. Hu, "Water Vapor Permeability of Cotton Fabrics Coated With Shape Memory Polyurethane," *Carbohydrate Polymers* 67 (2007): 282–287, https://doi.org/10.1016/j.carbpol.2006.05.030.

50. A. Walther, A. Bernhardt, W. Pompe, et al., "Development of Novel Scaffolds for Tissue Engineering by Flock Technology," *Textile Research Journal* 77 (2007): 892–899, https://doi.org/10.1177/0040517507081283.

51. A. R. P. D. Silva, T. L. Macedo, D. J. Coletta, S. Feldman, and M. D. M. J. M. Pereira, "Synthesis, Characterization and Cytotoxicity of Chitosan/Polyvinyl Alcohol/Bioactive Glass Hybrid Scaffolds Obtained by Lyophilization," *Materia-Rio De Janeiro* 21 (2016): 964–973, https://doi.org/10.1590/s1517-707620160004.0089.

52. J. E. Gough, C. A. Scotchford, and S. Downes, "Cytotoxicity of Glutaraldehyde Crosslinked Collagen/Poly (Vinyl Alcohol) Films is by the Mechanism of Apoptosis," *Journal of Biomedical Materials Research* 61 (2002): 121–130, https://doi.org/10.1002/jbm.10145.

Supporting Information

Additional supporting information can be found online in the Supporting Information section.

Supporting File 1: adma74548-sup-0001-SuppMat.docx.

Supporting File 2: adma74548-sup-0002-MovieS1.mp4.

Supporting File 3: adma74548-sup-0003-MovieS2.mp4.

Supporting File 4: adma74548-sup-0004-MovieS3.mp4.

Supporting File 5: adma74548-sup-0005-MovieS4.mp4.

Supporting File 6: adma74548-sup-0006-MovieS5.mp4.

Supporting File 7: adma74548-sup-0007-MovieS6.mp4.